

Dry Sliding Tribological Studies of AA6061-B₄C-Gr Hybrid Composites

V.V. Monikandan, M.A. Joseph, and P.K. Rajendrakumar

(Submitted June 23, 2015; in revised form July 5, 2016; published online August 25, 2016)

The dry sliding behavior of stir-cast AA6061-10 wt.% B₄C composites containing 2.5, 5 and 7.5 wt.% graphite particles was studied as a function of applied load, sliding speed and sliding distance on a pin-on-disk tribotester. The wear rate and friction coefficient increased with increase in applied load and sliding distance. The increase in graphite addition reduced the increase in wear rate and friction coefficient in the sliding speed range 2-2.5 m/s. Scanning electron microscopy of the worn pin revealed a graphite tribolayer, and transmission electron microscopy revealed overlapping deformation bands under 30 N applied load. Upon increasing the applied load to 40 N, welded region with fine crystalline structure was formed due to dynamic recrystallization of AA6061 alloy matrix.

Keywords AA6061-B₄C-Gr hybrid composites, deformation bands, dynamic recrystallization, tribolayer

1. Introduction

The need for high-performance materials in the defense sector has been the major motivation behind the development of metal matrix composites (MMCs) (Ref 1). The research and development of MMCs gained considerable significance in the early 1980s (Ref 2). The literature on B₄C-reinforced mono composites and hybrid composites is limited owing to the higher cost of B₄C particles compared to the conventional ceramic phases such as SiC (Ref 3) and Al₂O₃ particles (Ref 4). It is observed that the use of B₄C as a secondary phase provides significant specific property improvements for MMCs (Ref 3). Thus, in an earlier work, Monikandan et al. (Ref 5) fabricated an AA6061-10 wt.% B₄C mono composite through stir casting and reported its tribological properties.

Hybrid composites reinforced with solid lubricant particles provide solid lubrication by forming a tribolayer during sliding. The Gr (graphite)-reinforced composites are identified to be the potential materials for many commercial applications (Ref 6). The carbon atoms in the basal planes of Gr are held together by strong covalent bonds, but the basal planes themselves are held together by weak van der Waals forces resulting in interplanar mechanical weakness. Solid lubrication is imparted due to the interlamellar shearing of Gr, which is influenced by the presence of water vapor and crystal defects (Ref 7). The lubricity of Gr is not an intrinsic property (Ref 8), and if the testing environment lacks water vapor content, erratic friction behavior has resulted owing to the rapid disintegration of Gr into dustlike debris (Ref 9). The literature suggests that the Al-SiC-Gr hybrid composites exhibit better wear properties

compared to that of the Al-SiC mono counterparts (Ref 10-16). During statistical analysis of hybrid composites reinforced with Gr particles, the concentration of Gr acts as a significant factor which influences the wear loss (Ref 16, 17). Guo and Tsao (Ref 18) observed that the weight loss of Gr-reinforced hybrid composite was increased when Gr was added up to 5 vol.% beyond which the weight loss was decreased. In related work, Guo and Tsao (Ref 19) observed the same phenomenon for the Al-SiC-Ni-coated Gr hybrid composites. The literature on Al-SiC-Gr hybrid composites indicates that the friction coefficient decreases with increase in Gr addition, up to 13 vol.% (Ref 20). The decrease in friction coefficient up to 7.5 wt.% Gr addition and subsequent increase up to 10 wt.% Gr was also reported (Ref 21). Prabakaran et al. (Ref 22) compared the tribological properties of the AA6061 alloy, AA6061-10 wt.% B₄C mono composite and AA6061-10 wt.% B₄C-3 wt.% Gr hybrid composite; however, the work does not focus on the role of variation of Gr concentration in the tribological behavior of the hybrid composite.

The literature also indicates that the applied load and sliding speed may cause surface recrystallization and texture due to severe local deformation and surface temperatures (Ref 23). Sliding of stainless steel ring against an oxygen-free high conductivity (OFHC) Cu block at a sliding speed of 0.01 m/s and applied load of 67 N produced cell and subgrain substructure on the OFHC Cu block (Ref 24). Sliding of pure Cu against 440 C steel at an applied load of 10 N and sliding speed of 12.4 m/s produced fine-grained recrystallized region on the worn surface of pure Cu (Ref 25). Sliding of Al-Cu alloy against gray cast iron was observed to form small subgrains on Al-Cu alloy due to dynamic recrystallization (Ref 26).

The above literature makes it evident that the test parameters and conditions, Gr particle concentration and the formation of tribolayer influence the tribological properties of Gr-reinforced hybrid composites. Also, studies on hybrid composites with B₄C as ceramic phase are sparse. Studies on the development of fine-grained crystalline structures for hybrid composites are also lacking. Taking these facts into account, in the present study, hybrid composites of AA6061-10 wt.% B₄C-Gr with varying Gr particle concentration were fabricated through stir casting and were tested and characterized to understand the

V.V. Monikandan, M.A. Joseph, and P.K. Rajendrakumar, Department of Mechanical Engineering, National Institute of Technology, Calicut, Kerala 673601, India. Contact e-mails: saai.manikandan@gmail.com and p110059me@nitc.ac.in.

tribological behavior. Al-B₄C-Gr hybrid composites with better self-lubricating properties can be a potential substitute for Al-Si alloys and also for other composites which are currently in use for automotive components.

2. Fabrication of Composites

The following sections detail the materials and stir casting method used for fabricating hybrid composites.

2.1 Materials

AA6061 alloy (Mg-0.86, Si-0.67, Fe-0.19, Cu-0.21, Ti-0.018, Mn-0.04, Cr-0.05, Zn-0.004, B-0.003, Pb-0.001 and the rest Al by wt.%), supplied by M/s. Hindalco Ind. Ltd., India, is selected as the matrix material. B₄C particles (supplied by M/s. Bhukhanvala Ind. Pvt. Ltd., India) of 30- μ m average particle size (APS) and natural Gr particles (supplied by M/s. Sigma-Aldrich, India) of 45 μ m APS are used as the reinforcement particles.

2.2 Stir Casting Method

A typical stir casting equipment available in-house has been used to synthesize AA6061-10 wt.% B₄C-Gr hybrid composites reinforced with 2.5, 5 and 7.5 wt.% Gr particles. Particle rejection and sedimentation are observed during stir casting when the concentration of Gr exceeds 7.5 wt.%. The Gr addition beyond 5 wt.% to Al-SiC mono composite leads to a significant increase in wear (Ref 16), and hence, a hybrid composite with 5 wt.% Gr addition is used in the present work.

AA6061 alloy bars are heated in a furnace to 800 °C, and the melt temperature is maintained to a precision of ± 2 °C. The wettability of the reinforcement particles with the melt is enhanced by the addition of 1 wt.% magnesium (Mg). Hydrogen is removed by immersing hexachloroethane (C₂Cl₆) tablets into the melt. Granular cleaning flux is then added to remove the other non-metallic inclusions and oxides. The reinforcement particles are mixed in an aluminum agate mortar and pestle and preheated to 300 °C. The stirring speed is fixed at 450 rpm, and after addition of reinforcement particles mixture into the vortex, stirring is further continued for 1500 s. The composite melt is poured through the bottom pouring opening in the furnace, and after solidifying at atmospheric conditions, the hybrid composite is removed from the permanent mold.

3. Testing and Characterization Scheme

Details of the tribotest conditions and the characterization techniques used in the study are explained in the following sections.

3.1 Tribotests

A pin-on-disk tribotester (Ducom, TR-20 LE) was employed to test the composite pins of height 30 mm and diameter 8 mm. Dry sliding wear tests were conducted as per ASTM G99-05 Standard for applied loads of 10, 20, 30, 40 and 50 N, sliding speeds of 0.5, 1, 1.5, 2 and 2.5 m/s and sliding distances of 200, 400, 600, 800 and 1000 m. The track radius was selected

as 0.1 m, and tests were carried out under atmospheric conditions (1 atm., 30 ± 1 °C and $70 \pm 5\%$ RH) against the counterface, EN31 bearing steel disk of hardness 65 HRC and surface roughness of 0.1 μ m. The pin surface was polished using 600 grit SiC abrasive sheets to minimize the protrusion of ceramic particles. A finely polished pin surface promotes the micro-cutting of the counterface by the protruded ceramic particles at the beginning of sliding. Before each test, the tribopair was cleaned by acetone. The wear loss was quantified at a sensitivity of 0.1 mg using a precision balance. The wear rate is computed using the formula $W = \delta W/S$ where W is the wear rate in mg/m; δW is the difference in weight of the pin before and after the test in mg; and S is the sliding distance in m. The coefficient of friction was computed as the ratio of tangential friction force to the normal force. Each test was repeated three times to confirm the repeatability, and the mean of the three readings was taken to plot the graphs. Error bars indicate the standard deviation.

It is to be noted that the applied load range selected in this work is similar to the applied load range used to test the mono composite (Ref 5). In the case of the sliding speed and sliding distance, the selected values are 0.5, 1, 1.5 and 2 m/s and 200, 400, 600 and 800 m, respectively, for the mono composite (Ref 5). In this work, the test range is further extended to 2.5 m/s of sliding speed and 1000 m of sliding distance to compare the tribological properties of the mono composite with that of the hybrid composites.

3.2 Characterization

The distribution of reinforcement particles in the matrix alloy was analyzed using an optical microscope (OM, Qs metrology, XJL-17), and the worn pin surfaces were examined using scanning electron microscope (SEM, Hitachi, SU6600). Electron-dispersive x-ray spectroscopy (EDS, Horiba, EMAX 137 eV), high-resolution transmission electron microscope (HRTEM, Jeol, JEM-2100) and focused ion beam (FIB, Zeiss, Neon 40 EsB CrossBeam) milling were also used in the characterization of worn pin surfaces.

4. Results and Discussion

The metallographic analyses and the tribological behavior of the composites are discussed in the following sections:

4.1 Metallographic Analyses

The specimens are polished initially by SiC abrasive sheets followed by the diamond abrasive paste of grades 6, 3 and 1 μ m, respectively, on synthetic velvet clothes. Diamond extender is used as the lubricant, and the paste is replenished every few minutes. The polished surface is etched using Dix-Keller's reagent (2 mL hydrofluoric acid, 3 mL hydrochloric acid, 5 mL nitric acid and 190 mL distilled water) for an etching time of 15 s.

Metallographs of 2.5 and 5 wt.% Gr hybrid composites shown in Fig. 1(a) and (b) exhibit uniform dispersion of B₄C and Gr particles (marked with arrow). Micrographs of the mono composite are available in a previous work (Ref 5), and metallograph of the 7.5 wt.% Gr hybrid composite and its XRD spectrum are also available in an earlier work (Ref 17). XRD spectra of the 2.5 and 5 wt.% Gr hybrid composites (marked

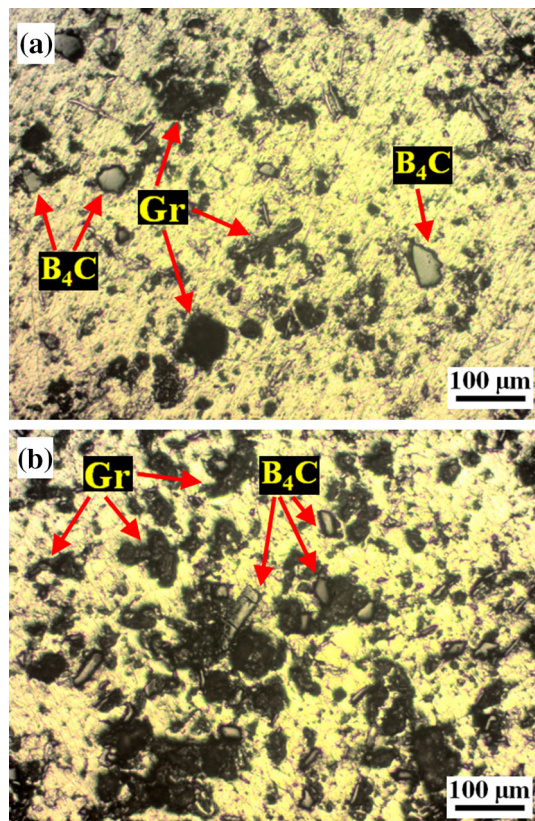


Fig. 1 Optical metallographs of the hybrid composites: (a) AA6061-10 wt.% B₄C-2.5 wt.% Gr and (b) AA6061-10 wt.% B₄C-5 wt.% Gr (B₄C and Gr particles are marked with arrow)

with dotted arrow) shown in Fig. 2 confirm the presence of B₄C and Gr particles in the hybrid composites, and it is also evident that the B₄C and Gr particles did not react with the matrix material.

4.2 Tribological Studies

In this section, the influence of sliding wear parameters and concentration of Gr particles on the tribological behavior is discussed.

4.2.1 Influence of Applied Load on Wear Rate. For sliding distance of 600 m and sliding speed of 1.5 m/s, the variation of wear rate has been plotted against applied load for different composites, as shown in Fig. 3. It is evident that the wear rate increases with increase in applied load for all the hybrid composites studied. At 10 N applied load, the junctions of contact asperities are shorn off, and the softer pin surface material is transferred onto the harder counterface. Small cavities (marked with dotted arrow) and shallow sliding grooves (marked with arrow) are observed on the worn pin surface as shown in Fig. 4. As the applied load increases, the Gr particles are exposed to sliding and start to smear on the contact surfaces. These particles along with the debris get mixed, comminuted and compacted at the tribopair interface leading to the formation of the tribolayer.

The formation of tribolayer is supported by the continuous flow of wear debris back and forth between the tribopair. Tribolayer formed on the worn pin surface of the 7.5 wt.% Gr hybrid composite has shallow sliding marks (marked with arrow) as shown in Fig. 5(a). Figure 5(b) shows the high

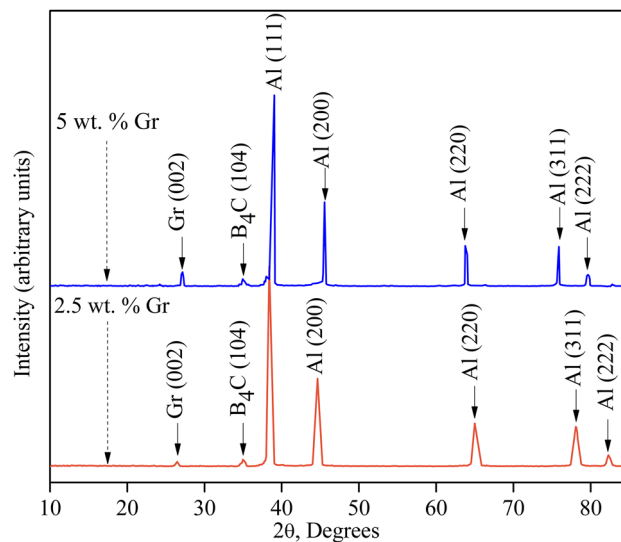


Fig. 2 XRD spectra of the AA6061-10 wt.% B₄C-2.5 wt.% Gr hybrid composite (marked with dotted arrow) and AA6061-10 wt.% B₄C-5 wt.% Gr hybrid composite (marked with dotted arrow)

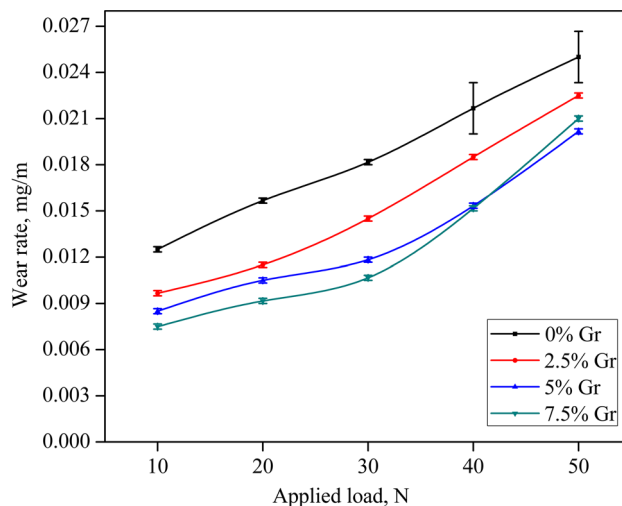


Fig. 3 Variation of wear rate with applied load for a sliding distance of 600 m and sliding speed of 1.5 m/s for the mono and 2.5, 5 and 7.5 wt.% Gr hybrid composites

magnification micrograph, and Fig 5(a) and (c) shows the backscattered electron (BSE) micrograph which reveals smeared Gr particles (marked with arrow) of the tribolayer. The chemical composition (Al 81.33, C 10.03, O 0.92, Mg 0.81, Si 0.47, Cr 0.33, Fe 6.01 and Cu 0.1 by wt.%) of the tribolayer is characterized using EDS spectrum. The iron (Fe) content in the tribolayer is 6.01 wt.% which is higher than the quantity of Fe present as the alloying element in the matrix material. This phenomenon is incurred due to the back and forth transfers of debris between the tribopair as a result of which the iron particles from the counterface get transferred to the pin surface. More evidence of transfer loops between the tribopair may be gathered from Fig. 6 which shows a cluster of debris inside a continuous groove. The debris could have moved through the groove and transferred from the interface during the transfer loops of the debris. EDS spectrum is used to characterize the debris clusters whose chemical composition

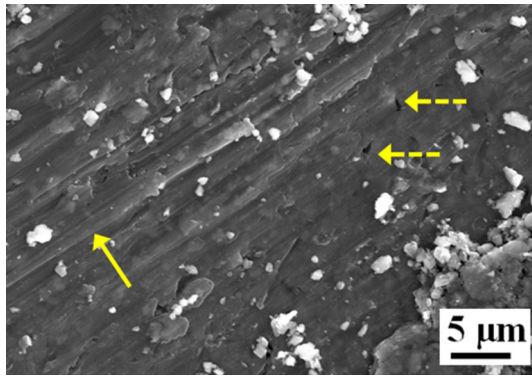


Fig. 4 SEM micrograph showing shallow sliding grooves (marked with arrow) and small cavities (marked with dotted arrow) on 2.5 wt.% Gr hybrid composite worn pin surface (applied load 10 N, sliding distance 600 m and sliding speed 1.5 m/s)

(Al 80.13, C 10.07, O 1.06, Mg 0.16, Si 0.26, Cr 0.09, Mn 0.03, Fe 8.13 and Cu 0.07 by wt.%) consists of the same elements as that of the tribolayer.

Further increase in applied load results in plastic deformation of the asperities on the worn pin surface that are made into contact with the counterface asperities. During sliding, dislocations are produced due to the plastic and micro-plastic deformation of the asperities of the worn pin surface (Ref 27). As the sliding continues, the dislocations get piled up and eventually voids and cracks are formed which results in the generation of platelet-shaped wear particles. Figure 7 shows the delaminated worn pin surface of the 2.5 wt.% Gr hybrid composite which reveals the presence of a platelet-shaped particle (marked with arrow).

It is seen from Fig. 3 that at the applied load of 50 N, 7.5 wt.% Gr hybrid composite exhibit higher wear rate than 5 wt.% Gr hybrid composite. This behavior may be attributed to the decrease in the fracture toughness of the 7.5 wt.% Gr hybrid composite due to the increase in Gr content. The Gr particles have a low strength which leads to the nucleation and propagation of cracks preferentially at the locations of cavities containing Gr particles (Ref 28). As the applied load increases, the advancing crack passes easily through the Gr particles which lead to the decrease in fracture toughness. The decrease in fracture toughness of the hybrid composites with the increase in Gr addition is observed in different studies (Ref 18, 19). Also, it is observed from Fig. 3 that the hybrid composites exhibit lesser wear rate than that of the mono composite due to the solid lubrication imparted by the tribolayer.

It is to be noted that the tribolayer formation does not reverse the trend of increase in wear rate with increase in applied load for all the hybrid composites studied. The Gr particles get continuously squeezed out to the contact surfaces and contribute to the wear rate. A monotonic increase in wear rate with increase in applied load is observed for Gr brushes sliding on a steel slip ring, even under lubrication provided by Gr (Ref 29). Further, increase in wear with the increase in applied load is observed by different authors for Gr-reinforced composites (Ref 11, 15, 16, 28).

4.2.2 Influence of Sliding Speed on Wear Rate. For sliding distance of 600 m and applied load of 30 N, the variation of wear rate has been plotted against sliding speed for the different composites, as shown in Fig. 8. It is observed that the wear rate of all the hybrid composites studied decreased

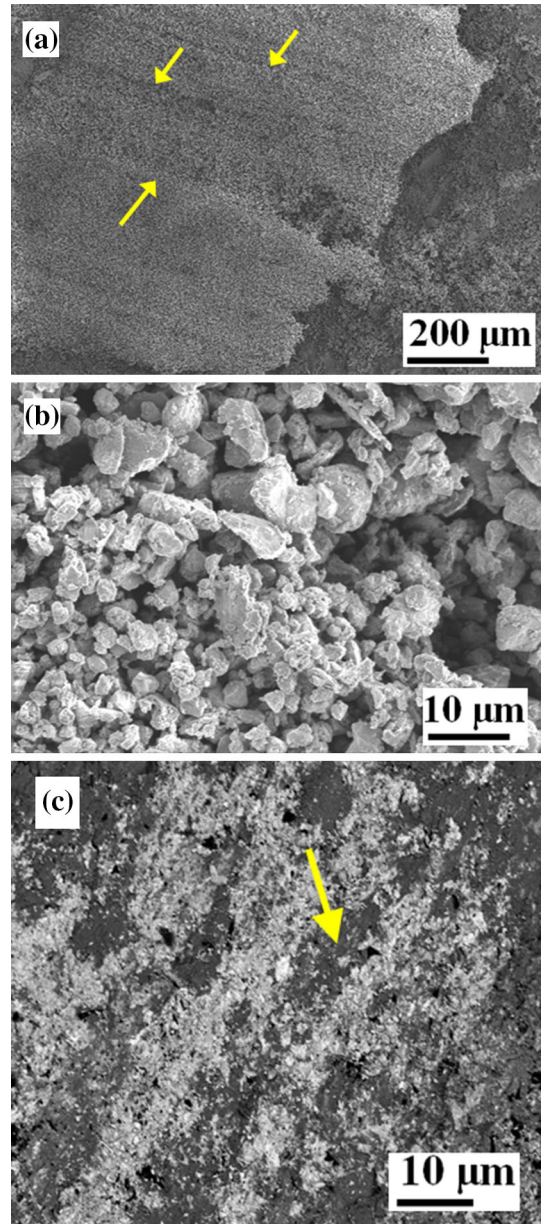


Fig. 5 SEM micrographs of tribolayer formed on 7.5 wt.% Gr hybrid composite worn pin surface: (a) low magnification micrograph showing shallow sliding marks (marked with arrow), (b) high magnification micrograph and (c) BSE micrograph showing smeared Gr particles (marked with arrow) (applied load 20 N, sliding distance 600 m and sliding speed 1.5 m/s)

with increase in sliding speed till 2 m/s, beyond which it increases. Two different factors influenced the decrease in wear rate: (1) the lubrication provided by tribolayer (Ref 30) and (2) increase in flow strength leading to the reduction in the real area of contact between the mating surfaces (Ref 31). However, increase in sliding speed beyond 2 m/s resulted in the increase in wear rate due to the increase in temperature caused by frictional heating. The rise in temperature leads to softening of the worn pin surface which undergoes plastic deformation (Ref 31).

A FIB/SEM instrument is used to characterize the plastically deformed surface of the 2.5 wt.% Gr hybrid composite specimen, obtained by milling a rectangular slot of 5 μm × 4

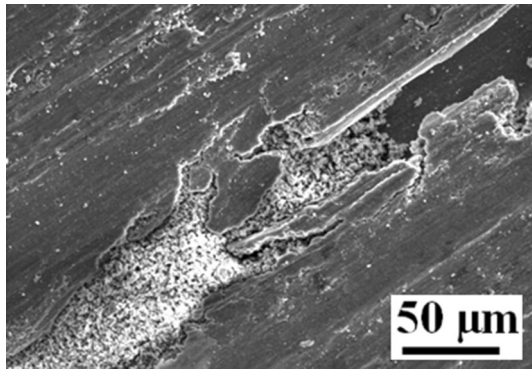


Fig. 6 SEM micrograph of the continuous groove with debris clusters on 7.5 wt.% Gr hybrid composite worn pin surface (applied load 20 N, sliding distance 600 m and sliding speed 1.5 m/s)

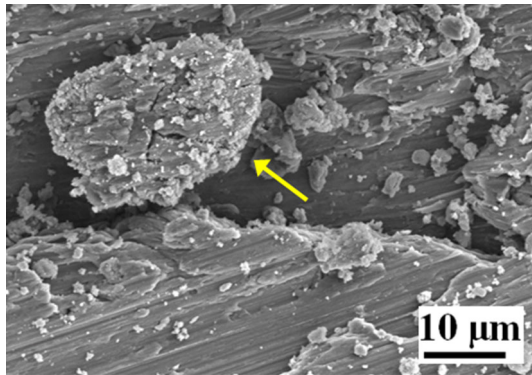


Fig. 7 SEM micrograph showing platelet-shaped particle (marked with arrow) on 2.5 wt.% Gr hybrid composite worn pin surface (applied load 50 N, sliding distance 600 m and sliding speed 1.5 m/s)

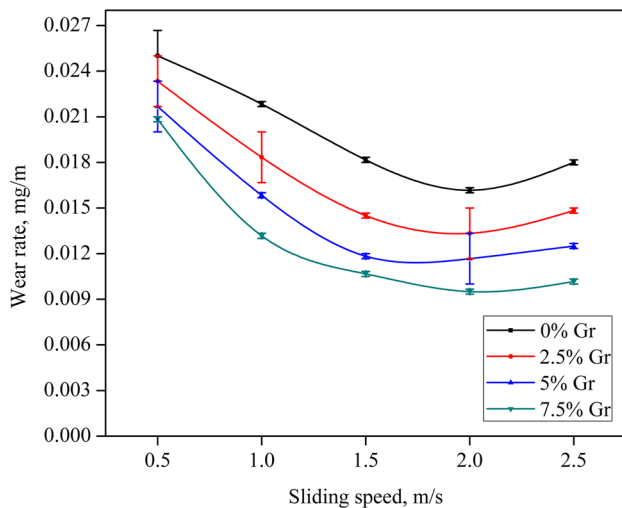


Fig. 8 Variation of wear rate with sliding speed for a sliding distance of 600 m and applied load of 30 N for the mono and 2.5, 5 and 7.5 wt.% Gr hybrid composites

$\mu\text{m} \times 3 \mu\text{m}$ depth in the direction perpendicular to that of sliding. The rectangular slot is milled using gallium (Ga) ion beam with an accelerating voltage of 30 keV and beam current, 2500 pA.

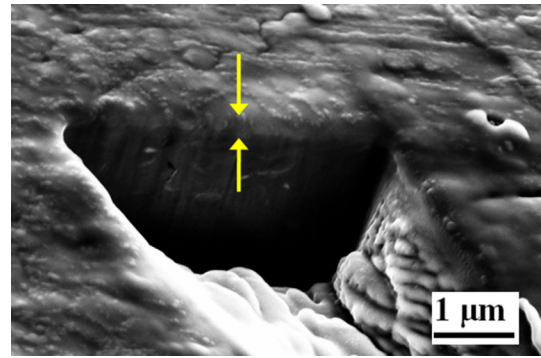


Fig. 9 SEM micrograph showing the deformed region (marked with arrow) on 2.5 wt.% Gr hybrid composite worn pin surface (sliding speed 2.5 m/s, sliding distance 600 m and applied load 30 N)

After milling, the cross section which is shown in Fig. 9 is imaged by tilting the SEM stub to an angle 56° . The thickness of the deformed region (marked with arrow) is about 233 nm (rounded off value). The plastic deformation would have led to delamination of the worn pin surface, giving rise to the formation of wear debris (Ref 32). The wear debris produced at this stage consists of a combination of delaminated platelet-shaped particles [marked with dotted arrow in Fig. 10(a) and (b)] and debris lumps (marked with arrow) as shown in Fig. 10(b). Figure 10(c) shows a highly magnified image of the platelet-shaped debris of Fig. 10(b) which reveals cross-hatchings (marked with arrow) along its surface. Cross-hatchings serve as the precursor from which platelet-shaped particles are formed and get detached (Ref 33).

In the case of the mono and 7.5 wt.% Gr hybrid composites increase in wear rate of about 11 and 4% (rounded off value), respectively, has been observed as the sliding speed is increased from 2 to 2.5 m/s. The plastic deformation is decreased with an increase in the wt.% addition of Gr particles (Ref 34), and also, due to increase in Gr content, there is a considerable increase in adherence of sheared Gr lamellae on the worn pin surface which covers the wear track to provide some lubrication. These are the prime factors to mitigate the increase in wear rate for 7.5 wt.% Gr hybrid composite. In the case of the mono composite, the decrease in wear rate up to the sliding speed of 2 m/s is due to the formation of mechanically mixed layer (MML) (Ref 5) which goes unstable as the sliding speed increases to 2.5 m/s leading to the increase in wear rate.

4.2.3 Influence of Sliding Distance on Wear Rate. For a sliding speed of 1.5 m/s and applied load of 30 N, the variation of wear rate has been plotted against sliding distance for the different composites as shown in Fig. 11. It is observed that the wear rate increases with increase in sliding distance for all the hybrid composites studied. Also, it is inferred that the wear rate of 2.5, 5 and 7.5 wt.% Gr hybrid composites is less than that of its mono counterpart. This behavior is attributed to the Gr particles which get squeezed onto the contact surface to provide solid lubrication. However, lubrication is not effective enough to reverse the trend of increasing wear rate. As the sliding distance increases, higher shear strain is induced in the subsurface region which is further increased in regions close to the pin surface. Also, the magnitude of the shear strain increases with increase in sliding distance. The subsurface region and regions close to the pin surface which are induced

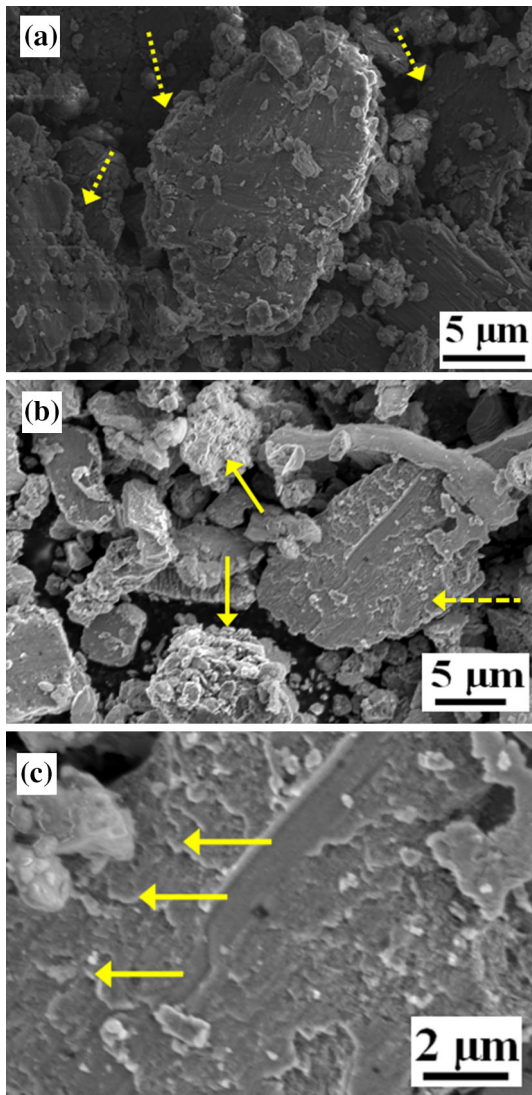


Fig. 10 SEM micrographs of 2.5 wt.% Gr hybrid composite wear debris: (a) platelet-shaped particles (marked with dotted arrow), (b) combination of debris lumps (marked with arrow) and platelet-shaped particle (marked with dotted arrow) and (c) cross-hatchings (marked with arrow) (sliding speed 2.5 m/s, sliding distance 600 m and applied load 30 N)

with the shear strain undergoes plastic deformation causing the tribolayer of the hybrid composites to delaminate leading to its disintegration. Figure 12 shows disintegrated tribolayer on the worn pin surface of 5 wt.% Gr hybrid composite at 800 m of sliding distance. The tribolayer retains its structural integrity in a small region (marked A), and for the rest of the region, it is disintegrated into tiny particle clusters (marked with arrow). The weakening of the tribolayer with the increase in sliding distance was also reported for Al-SiC-Gr composites (Ref 30).

The dispersed wear debris combined with the B₄C particles that are removed from the deformed zone micro-ploughs the tribopair. As the micro-ploughing continues with the increase in sliding distance, the worn pin surface gets cracked and bulged upwards (marked with dotted arrow) as shown in Fig. 13(a). Figure 13(b) shows the continuous crack (marked with arrow) as well as the damaged material at the surrounding regions of the continuous crack which has bulged upwards (marked with

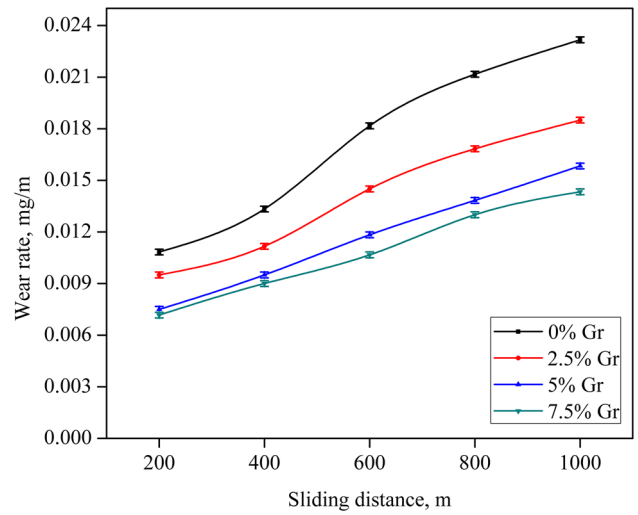


Fig. 11 Variation of wear rate with sliding distance for a sliding speed of 1.5 m/s and applied load of 30 N for the mono and 2.5, 5 and 7.5 wt.% Gr hybrid composites

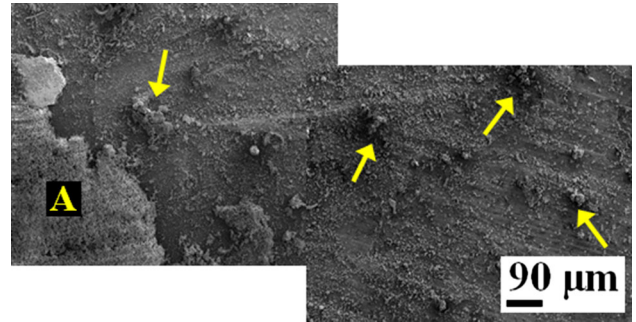


Fig. 12 SEM micrograph showing the disintegration of tribolayer into particle clusters (marked with arrow) and the presence of tribolayer in a small region (marked A) on 5 wt.% Gr hybrid composite worn pin surface (sliding distance 800 m, sliding speed 1.5 m/s and applied load 30 N)

dotted arrow). Numerous shallow cracks (marked with open arrow) running in the direction transverse to that of the continuous crack are also observed in Fig. 13(b). Figure 13(a) and (b) distinguishes between the short and continuous cracks at two different locations of the worn pin surface.

The wear debris produced at this stage is mostly thin and curled as shown in Fig. 14(a). Figure 14(b) shows the debris with cleaved circumferential edges which are formed probably due to micromachining of the matrix material by the fractured B₄C particles, and Fig. 14(c) shows the curved debris which exhibits shallow sliding marks (marked with arrow).

4.2.4 Influence of Applied Load on Friction Coefficient. For sliding distance of 600 m and sliding speed of 1.5 m/s, the variation of friction coefficient has been plotted against applied load for the different composites, as shown in Fig. 15. It is observed that the friction coefficient increases with increase in applied load for all the hybrid composites studied. It is to be noted that the wear mechanisms influence the state of the pin surface which in turn affects friction (Ref 35). Since the pin surface is not fine polished, the matrix material and the counterface constitute the contact surfaces. At the applied load of 10 N, adhesion leads to increase in friction coefficient as the

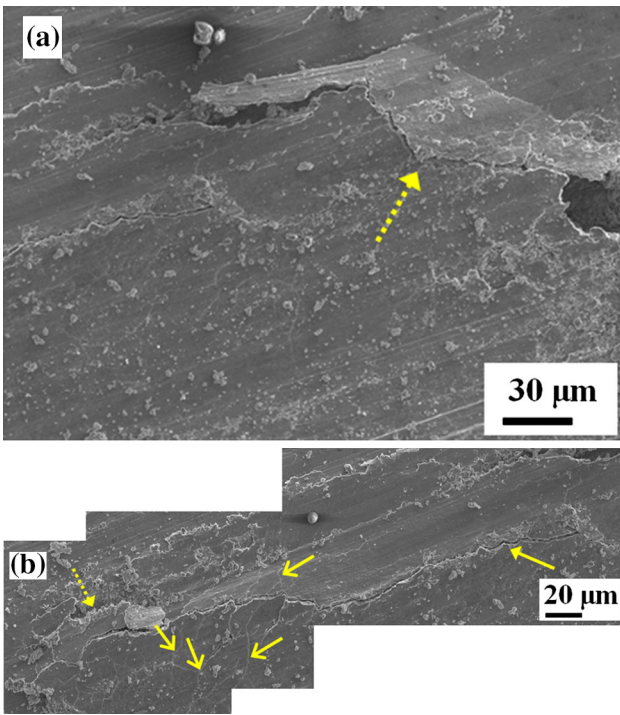


Fig. 13 SEM micrographs of 5 wt.% Gr hybrid composite worn pin surface: (a) upward bulging of cracked material (marked with dotted arrow) and (b) continuous crack (marked with arrow), shallow cracks (marked with open arrow) and damaged material surrounding the continuous crack (marked with dotted arrow) (sliding distance 1000 m, sliding speed 1.5 m/s and applied load 30 N)

ductile matrix material is transferred to the counterface. At 20 N applied load, the tribolayer formed covers the protruded B_4C particles. As the applied load increases, B_4C particles press against the tribolayer on the worn pin surface to break and loosen it leading to the formation of regions without tribolayer. The wear debris which is rich in fine reinforcement particles gets transferred to the counterface which is very rough and wavy.

So, the transferred debris cannot cover the counterface asperities, and they come in direct metallic contact with the worn pin surface in regions where the tribolayer is depleted. This phenomenon also contributes to the increase in friction coefficient, and at the applied load of 50 N, delaminated debris get clogged between the tribopair surfaces to increase the friction coefficient further. It is inferred from Fig. 15 that the friction coefficient of the mono composite increases with increase in applied load. This behavior is linked to the adhesion at low applied loads, and the B_4C particles influence the friction coefficient significantly as the applied load increases (Ref 5). Also, the friction coefficient of the mono composite is higher than that of the hybrid composites due to the absence of solid lubricant phase.

4.2.5 Influence of Sliding Speed on Friction Coefficient. For applied load of 30 N and sliding distance of 600 m, the variation of friction coefficient has been plotted against sliding speed for the different composites as shown in Fig. 16.

It is observed that the friction coefficient of the hybrid composites is decreased with increase in sliding speed up to 2 m/s due to the lubrication imparted by the tribolayer. As the

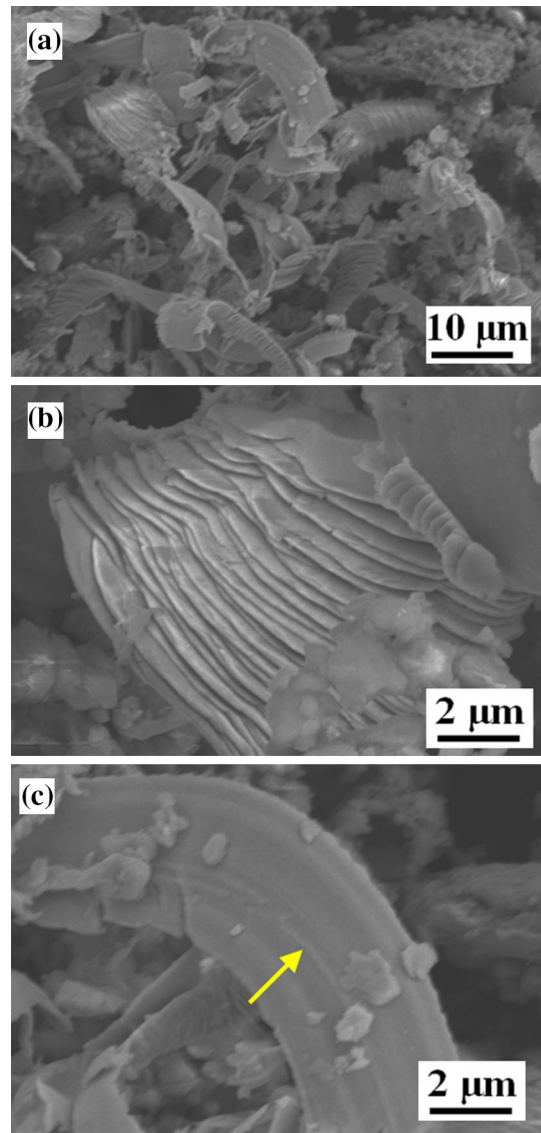


Fig. 14 SEM micrographs of 5 wt.% Gr hybrid composite wear debris: (a) thin and curled debris, (b) debris with cleaved circumferential edges and (c) curved debris with shallow sliding marks (marked with arrow) (sliding distance 1000 m, sliding speed 1.5 m/s and applied load 30 N)

sliding speed increases from 2 to 2.5 m/s, increase in wear rate is observed due to delamination. Delaminated debris slides in between the contact surfaces and causes damage on the pin surface which leads to an increase in friction coefficient. The observation of the increase in wear rate and the corresponding increase in friction coefficient is in agreement with the results reported by Ma and Lu (Ref 36) for Cu-Gr composites for the sliding speed range of 0.001-8 m/s. In the case of the mono composite, the formation of MML reduces the friction coefficient for sliding speeds up to 2 m/s (Ref 5). For the sliding speed range of 2-2.5 m/s, increase in friction coefficient observed for the 7.5 wt.% Gr hybrid composite is lower than that of the mono composite due to the presence of thin Gr lamellae.

4.2.6 Influence of Sliding Distance on Friction Coefficient. For applied load of 30 N and sliding speed of 1.5 m/s, the variation of friction coefficient has been plotted against

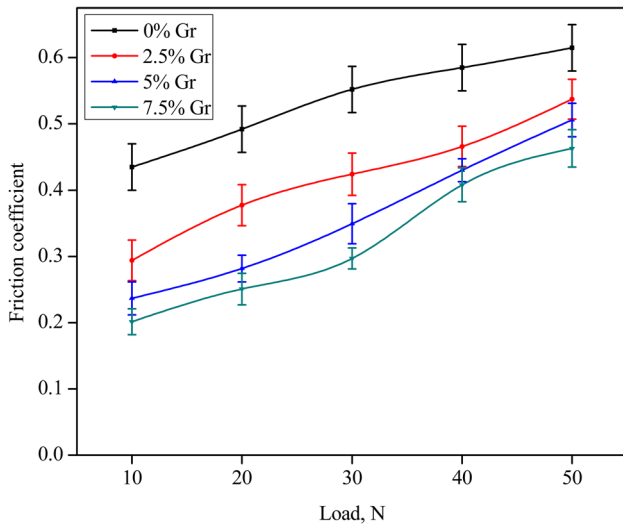


Fig. 15 Variation of friction coefficient with applied load for a sliding distance of 600 m and sliding speed of 1.5 m/s for the mono and 2.5, 5 and 7.5 wt.% Gr hybrid composites

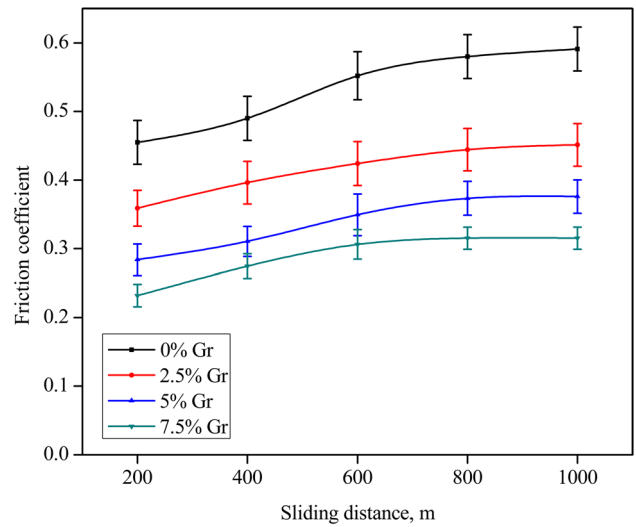


Fig. 17 Variation of friction coefficient with sliding distance for a sliding speed of 1.5 m/s and applied load of 30 N for the mono and 2.5, 5 and 7.5 wt.% Gr hybrid composites

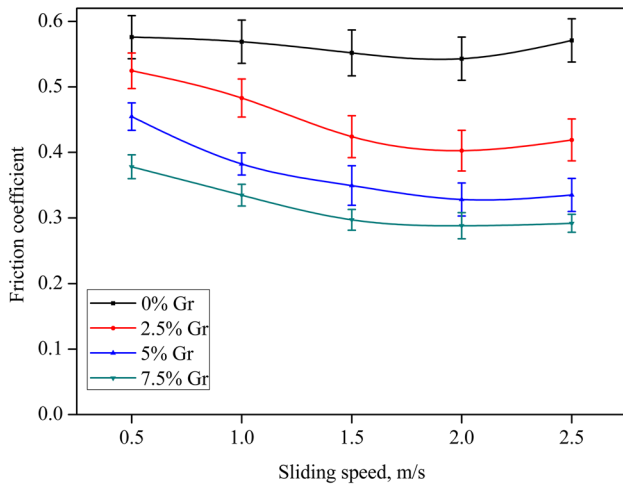


Fig. 16 Variation of friction coefficient with sliding speed for a sliding distance of 600 m and applied load of 30 N for the mono and 2.5, 5 and 7.5 wt.% Gr hybrid composites

sliding distance for the different composites as shown in Fig. 17. It is observed that the friction coefficient increases with increase in sliding distance for all the hybrid composites studied. As the sliding distance increases, subsurface plastic deformation causes disintegration of the tribolayer. Tsuya (Ref 37) considered the subsurface plastic deformation to be a significant phenomenon which influences the friction force and formulated a model of friction force, based on the subsurface plastic deformation. Abrasion of B_4C particles on the contact surfaces also leads to the increase in friction coefficient. Abrasion on the counterface by B_4C particles produce counterface debris as shown in Fig. 18.

EDS spectrum is used to characterize the chemical composition (Fe 96.9 and Al 3.1 by wt.%) of the counterface debris, and the dominant constituent is seen to be Fe. In the case of the mono composite, the subsurface deformation demoted the formation and sustenance of MML which causes the increase in friction coefficient with the increase in sliding distance (Ref 5).

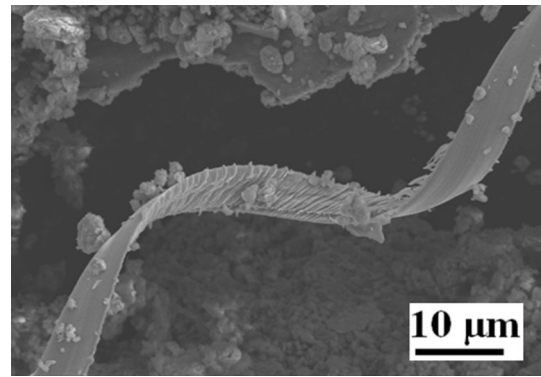


Fig. 18 SEM micrograph showing counterface debris (sliding distance 1000 m, sliding speed 1.5 m/s and applied load 30 N)

4.2.7 TEM Characterization of Worn Pin Surfaces.

Once sliding is initiated, friction is developed between the microscopic contact asperities and the conditions of sliding wear produces large strains and gross plastic deformation causing a series of deformation bands. The deformation bands become prominent with the occurrence of dynamic recovery (Ref 38). When the grains are unstable due to their crystallographic orientation, deformation bands are formed as the unstable grains get divided into coarse bands (Ref 39). Figure 19 shows the deformation bands overlapping one over the other and severe dislocation density (marked with dotted arrow). Gottstein et al. (Ref 40) indicated that the dynamic recrystallization could be initiated by extensive dynamic recovery if the dislocation density was high.

The increase in applied load causes severe localized heat and deformation, which thermally softens the pin surface to undergo dynamic recovery and dynamic recrystallization subsequently. While the dynamic recovery favors the formation of deformation bands and facilitates the redistribution of dislocations within the band to reduce the stored energy (Ref 41), the dynamic recrystallization may reduce the hardness of the 7.5 wt.% Gr hybrid composite and cause grain fragmen-

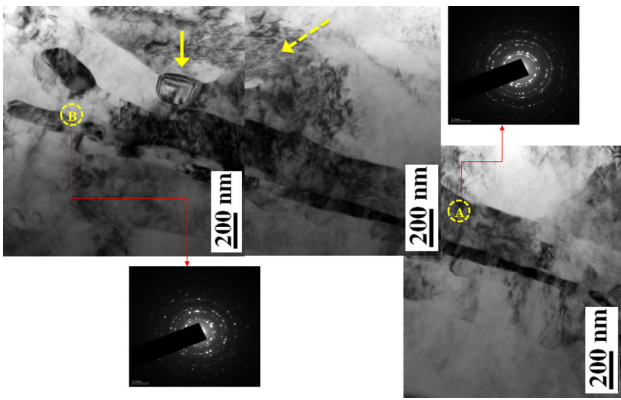


Fig. 19 TEM micrograph showing overlapping deformation bands, severe dislocation density (marked with dotted arrow) and thickness fringes (marked with arrow) on 7.5 wt.% Gr hybrid composite worn pin surface (applied load 30 N, sliding distance 600 m and sliding speed 1.5 m/s)

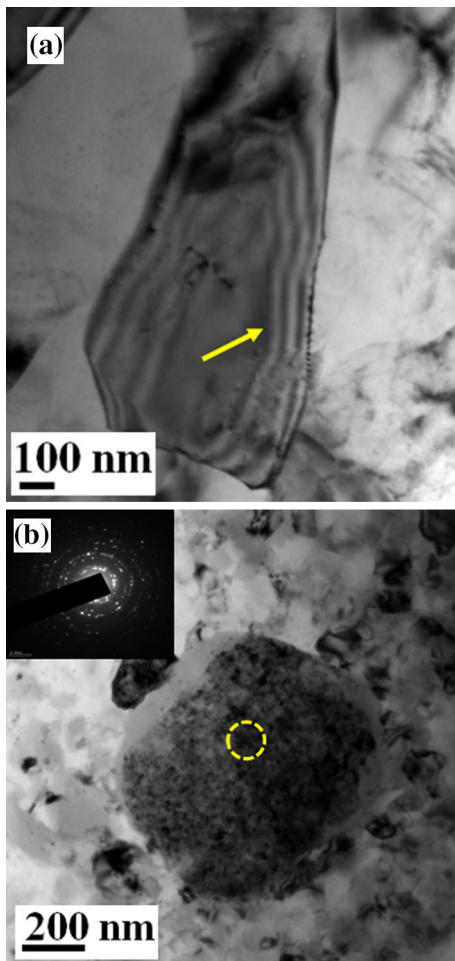


Fig. 20 TEM micrographs of 7.5 wt.% Gr hybrid composite worn pin surface: (a) extinction contours (marked with arrow) and (b) welded region (applied load 40 N, sliding distance 600 m and sliding speed 1.5 m/s)

tation at the band intersections. The selected area diffraction (SAD) patterns of the band (marked A) and band intersection (marked B) shown in Fig. 19 are ring-type patterns having

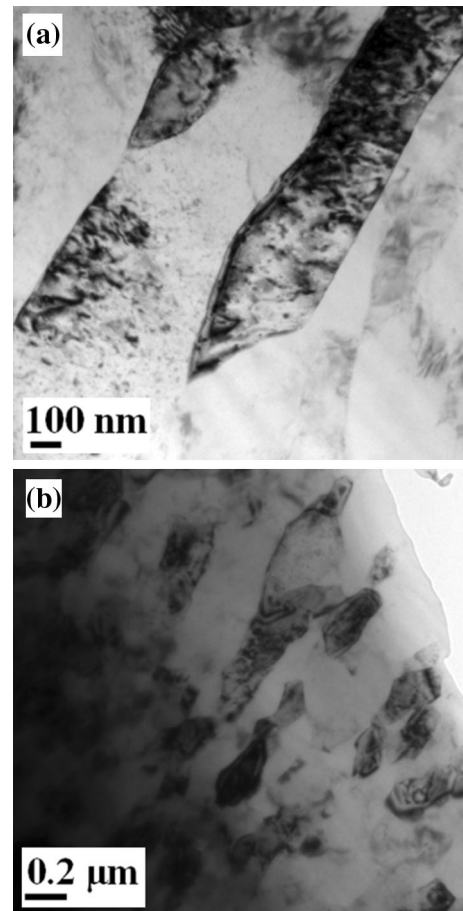


Fig. 21 TEM micrographs of 7.5 wt.% Gr hybrid composite worn pin surface: (a) Gr particles at applied load 10 N and (b) smearing of Gr particles at applied load 50 N (sliding distance 600 m and sliding speed 1.5 m/s)

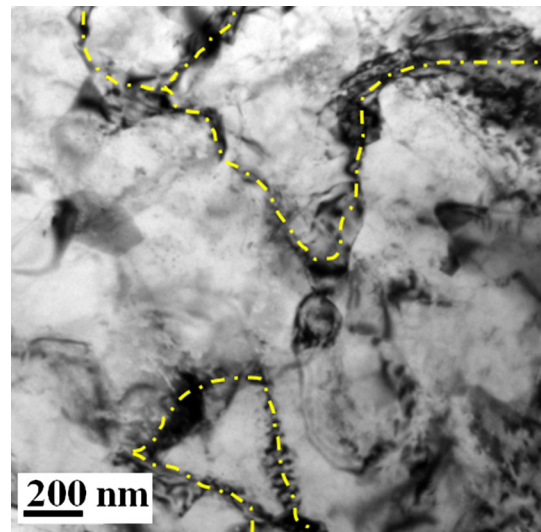


Fig. 22 TEM micrograph showing cell walls (traced with dotted line) on 7.5 wt.% Gr hybrid composite worn pin surface (applied load 50 N, sliding distance 600 m and sliding speed 1.5 m/s)

discrete spots which reveal the formation of fine crystalline structure. The formation of the fine crystalline structure is attributed to the phenomenon of dynamic recrystallization.

Using SAD patterns, Dautzenberg (Ref 42) observed dynamically recrystallized fine grains of worn Cu when Cu pins were subjected to dry sliding against steel ring. Emge et al. (Ref 43) observed dynamically recrystallized submicron-sized grains on OFHC copper disk which is subjected to sliding against stainless steel ball at a sliding speed of 1 m/s. Also, evidence of dynamic recrystallization of Al alloys was reported by some authors (Ref 44-46). Factors such as the composition of the matrix material, type of reinforcement particles, the hardness of composite and grain boundary defects influence the formation of the fine crystalline structure. Figure 19 also shows thickness fringes (marked with arrow) which are a phase-contrast phenomenon and give an appearance of a small corner-chamfered slot.

As the applied load increases to 40 N, relatively smooth extinction contours (marked with arrow) are observed on grain as shown in Fig. 20(a). Further, welding of the pin material over the counterface takes place, and the deformation is so severe that some material eventually gets welded back on to the worn pin surface as shown in Fig. 20(b). The SAD pattern of the welded region (marked with dotted circle) shows ring-type pattern [upper right inset of Fig. 20(b)] which reveals the formation of fine crystalline structure.

Figure 21(a) shows the Gr particles when the applied load is 10 N. As the applied load is increased to 50 N, the Gr particles get smeared as shown in Fig. 21(b). The high stress applied to the contact surface of the pin gradually changes its original microstructure to a cellular one which is capable of tolerating large strains in the direction of sliding. The cells are dislocation-free elements divided by the cell walls (traced with dotted line in Fig. 22) and firmly rotated relative to the neighboring material. It is to be noted that the reinforcement particles impede the movement of dislocations, contributing to the increase in stress required for initiating the dislocation movement which in turn leads to an increase in strength of the composite. Parallel dislocations tread one another on the same glide plane and form high-energy dislocation pileup structures as the hard reinforcement particles contain the dislocation. However, as the applied load is increased, the dislocation pileup stress exceeds its critical value, leading to the formation of micro-cracks and subsequent generation of wear debris. At this stage, the generation of adhesion-induced welded regions is ceased as wear is continued due to the propagation of micro-cracks developed in the vicinity of the fractured reinforcement particles.

5. Conclusions

In summarizing, the following inferences can be made from the experimental work:

- The wear rate of hybrid composites increases with increase in applied load. At the applied load of 10 N, adhesion is the wear mechanism, and as the applied load is increased to 50 N, delamination is induced. For the entire range of applied loads studied, the wear rate of the hybrid composites is less than that of the mono composite due to the solid lubrication imparted by the tribolayer.
- For the hybrid composites, the variation of wear rate with sliding speed depends on the formation of tribolayer which remains intact till 2 m/s to provide solid lubrication.

The wear rate is increased when the sliding speed is increased to 2.5 m/s, due to plastic deformation.

- In the case of the hybrid composites, for sliding speed of 2-2.5 m/s, the increase in wear rate and friction coefficient is lower than that of the mono composite due to the lubrication provided by the sheared Gr lamellae.
- The friction coefficient increases with applied load for the hybrid composites studied, due to the sequential occurrence of adhesion, depletion of the tribolayer and clogging of delaminated debris between the contact surfaces.
- The fine crystalline structure of the deformation bands, band intersections and welded region on the worn pin surface is indicative of dynamic recrystallization.

Acknowledgments

The authors thank Dr. T.P.D. Rajan, CSIR-NIIST, for his helpful suggestions on composites fabrication, Dr. Manoj Raama Varma of that same institute for TEM sample preparation, Mr. D. Aloysius Daniel, Nano Manufacturing Technology Center, CMTI, for the assistance during FIB milling and Mr. Vijaya Ragavan, PSG Institute of Advanced Studies, for the assistance during HRTEM characterization.

References

1. D.B. Miracle, Metal Matrix Composites—From Science to Technological Significance, *Compos. Sci. Technol.*, 2005, **65**, p 2526–2540
2. A. Evans, C.S. Marchi, A. Mortensen, *Metal Matrix Composites in Industry: An Introduction and A Survey*, 1st edn. (Kluwer, Waltham, 2003), chap. I, p 5
3. A.R. Kennedy, The Microstructure and Mechanical Properties of Al-Si-B₄C Metal Matrix Composites, *J. Mater. Sci.*, 2002, **37**, p 317–323
4. A. Canakci and F. Arslan, Abrasive Wear Behaviour of B₄C Particle Reinforced Al2024 MMCs, *Int. J. Adv. Manuf. Technol.*, 2012, **63**(5–8), p 785–795
5. V.V. Monikandan, M.A. Joseph, P.K. Rajendrakumar, and M. Sreejith, Tribological Behavior of Liquid Metallurgy-Processed AA 6061-B₄C Composites, *Mater. Res. Express*, 2015, **2**(1), p 1–11
6. S.V. Prasad and R. Asthana, Aluminium Metal-Matrix Composites for Automotive Applications: Tribological Considerations, *Tribol. Lett.*, 2004, **17**(3), p 445–453
7. S.V. Prasad, Friction and Wear Applications of Composites, *Concise Encyclopedia of Composite Materials*, 2nd ed., A. Kelly, Ed., Elsevier Science, Amsterdam, 1994, p 106–111
8. R.H. Savage, Graphite Lubrication, *J. Appl. Phys.*, 1948, **19**(1), p 1–10
9. D. Ramadanoff and S.W. Glass, High-Altitude Brush Problem, *Trans. Am. Inst. Electr. Eng.*, 1944, **63**, p 825–830
10. S. Suresha and B.K. Sridhara, Wear Characteristics of Hybrid Aluminium Matrix Composites Reinforced with Graphite and Silicon Carbide Particulates, *Compos. Sci. Technol.*, 2010, **70**, p 1652–1659
11. P. Ravindran, K. Manisekar, P. Rathika, and P. Narayanasamy, Tribological Properties of Powder Metallurgy-Processed Aluminium Self Lubricating Hybrid Composites with SiC Additions, *Mater. Des.*, 2013, **45**, p 561–570
12. S. Basavarajappa, G. Chandramohan, A. Mahadevan, M. Thangavelu, R. Subramanian, and P. Gopalakrishnan, Influence of Sliding Speed on the Dry Sliding Wear Behaviour and the Subsurface Deformation on Hybrid Metal Matrix Composite, *Wear*, 2007, **262**, p 1007–1012
13. A.R. Riahi and A.T. Alpas, The Role of Tribo-Layers on the Sliding Wear Behavior of Graphitic Aluminum Matrix Composites, *Wear*, 2001, **251**, p 1396–1407
14. L. Jinfeng, J. Longtao, W. Gaohui, T. Shoufu, and C. Guoqin, Effect of Graphite Particle Reinforcement on Dry Sliding Wear of SiC/Gr/Al Composites, *Rare Met. Mater. Eng.*, 2009, **38**(11), p 1894–1898
15. S. Basavarajappa, G. Chandramohan, K. Mukund, M. Ashwin, and M. Prabu, Dry Sliding Wear Behavior of Al 2219/SiC_p-Gr Hybrid Metal Matrix Composites, *J. Mater. Eng. Perform.*, 2006, **15**, p 668–674

16. P. Ravindran, K. Manisekar, P. Narayanasamy, N. Selvakumar, and R. Narayanasamy, Application of Factorial Techniques to Study the Wear of Al Hybrid Composites with Graphite Addition, *Mater. Des.*, 2012, **39**, p 42–54
17. V.V. Monikandan, J.C. Jacob, M. A. Joseph, P. K. Rajendrakumar, Statistical Analysis of Tribological Properties of Aluminum Matrix Composites Using Full Factorial Design, in *International Conference on Manufacturing and Materials Engineering (ICMME)*, Kanjirappally, Kerala, July, 2015, accepted
18. M.L.T. Guo and C.-Y.A. Tsao, Tribological Behavior of Self-Lubricating Aluminium/SiC/Graphite Hybrid Composites Synthesized by the Semi-Solid Powder Densification Method, *Compos. Sci. Technol.*, 2000, **60**, p 65–74
19. M.L.T. Guo and C.-Y.A. Tsao, Tribological Behavior of Aluminum/SiC/Nickel-Coated Graphite Hybrid Composites, *Mater. Sci. Eng. A*, 2002, **333**, p 134–135
20. S. Mahdavi and F. Akhlaghi, Effect of the Graphite Content on the Tribological Behaviour of Al/Gr and Al/30SiC/Gr Composites Processed by In Situ Powder Metallurgy (IPM) Method, *Tribol. Lett.*, 2011, **44**, p 1–12
21. S. Suresha and B.K. Sridhara, Friction Characteristics of Aluminium Silicon Carbide Graphite Hybrid Composites, *Mater. Des.*, 2012, **34**, p 576–583
22. S. Prabakaran, G. Chandramohan, and P. Shanmugasundaram, Influence of Graphite on the Hardness and Wear Behavior of AA6061-B₄C Composite, *Mater. Technol.*, 2014, **48**(5), p 661–667
23. D.H. Buckley and R.L. Johnson, The Influence of Crystal Structure and Some Properties of Hexagonal Metals on Friction and Adhesion, *Wear*, 1968, **11**(6), p 405–419
24. D.A. Rigney, M.G.S. Naylor, and R. Divakar, Low Energy Dislocation Structures Caused by Sliding and by Particle Impact, *Mater. Sci. Eng.*, 1986, **81**, p 409–425
25. R.C. Bill and D. Wisander, Recrystallization as a Controlling Process in the Wear of Some F.C.C. Metals, *Wear*, 1977, **41**, p 351–363
26. C. Perrin and W.M. Rainforth, The Effect of Alumina Fibre Reinforcement on the Wear of An Al-4.3 % Cu Alloy, *Wear*, 1995, **181–183**, p 312–324
27. N.P. Suh, The Delamination Theory of Wear, *Wear*, 1973, **25**, p 111–124
28. Y. Zhan and G. Zhang, Friction and Wear Behavior of Copper Matrix Composites Reinforced with SiC and Graphite Particles, *Tribol. Lett.*, 2004, **17**(1), p 91–98
29. J.E. Thompson and M.J.B. Turner, Mechanisms of the Wear of Graphite Sliding on Steel-with and without an Electric Contact Painting Across the Interface, *Nature*, 1962, **196**, p 329–331
30. S. Suresha and B.K. Sridhara, Effect of Addition of Graphite Particulates on the Wear Behaviour in Aluminium-Silicon Carbide-Graphite composites, *Mater. Des.*, 2010, **31**, p 1804–1812
31. C. Subramanian, Effects of Sliding Speed on the Unlubricated Wear Behaviour of Al-12.3 wt. % Si Alloy, *Wear*, 1991, **151**, p 97–110
32. Y.B. Liu, S.C. Lim, S. Ray, and P.K. Rohatgi, Friction and Wear of Aluminium-Graphite Composites: The Smearing Process of Graphite During Sliding, *Wear*, 1992, **159**, p 201–205
33. R.G. Bayer and R.A. Schumacher, On the Significance of Surface Fatigue in Sliding Wear, *Wear*, 1968, **12**(3), p 173–183
34. S.K. Biswas and B.N.P. Bai, Dry Wear of Al-Graphite Particle Composites, *Wear*, 1981, **68**, p 347–358
35. P.J. Blau, *The Effects of Tribosystem Variables on Frictional Response, Friction Science and Technology*, Marcel Dekker, New York, 1996, p 348
36. W. Ma and J. Lu, Effect of Sliding Speed on Surface Modification and Tribological Behaviour of Copper-Graphite Composite, *Tribol. Lett.*, 2011, **41**, p 363–370
37. Y. Tsuya, “Microstructures of Wear, Friction and Solid Lubrication,” Technical report no. 81. Mechanical Engineering Laboratory, Igusa Suginami-ku, Tokyo, 1976
38. C.S. Lee, B.J. Duggan, and R.E. Smallman, A Theory of Deformation Banding in Cold Rolling, *Acta Metall. Mater.*, 1993, **41**(8), p 2265–2270
39. P.J. Apps, M. Berta, and P.B. Prangnell, The Effect of Dispersoids on the Grain Refinement Mechanisms during Deformation of Aluminium Alloys to Ultra-High Strains, *Acta Mater.*, 2005, **53**, p 499–511
40. G. Gottstein, T. Lee, and U. Schmidt, Deformation Temperature and Recrystallization, *Mater. Sci. Eng. A*, 1989, **15**, p 21–28
41. C.S. Lee, R.E. Smallman, and B.J. Duggan, Deformation Banding and Formation of Cube Volumes in Cold Rolled FCC Metals, *Mater. Sci. Technol.*, 1994, **10**(10), p 862–868
42. J.H. Dautzenberg, The Role of Dynamic Recrystallization in Dry Sliding Wear, *Wear*, 1980, **60**, p 401–411
43. A. Emge, S. Karthikeyan, and D.A. Rigney, The Effects of Sliding Velocity and Sliding Time on Nanocrystalline Tribolayer Development and Properties in Copper, *Wear*, 2009, **209**(267), p 562–567
44. P. Faivre and R.D. Doherty, Nucleation of Recrystallization in Compressed Aluminium: Studies by Electron Microscopy and Kikuchi Diffraction, *J. Mater. Sci.*, 1979, **14**(4), p 897–919
45. H.J. McQueen, O. Knustad, N. Ryum, and J.K. Solberg, Microstructural Evolution in Al Deformed to Strains of 60 at 400 °C, *Scr. Metall.*, 1985, **19**(1), p 73–78
46. S.M. Kuo and D.A. Rigney, Sliding Behaviour of Aluminum, *Mater. Sci. Eng. A*, 1992, **157**(2), p 131–143